Acta Cryst. (1981). A**37**, 594–604

Improved Technique for Peak Integration for Crystallographic Data Collected with Position-Sensitive Detectors: A Dynamic Mask Procedure

BY LENNART SJÖLIN AND ALEXANDER WLODAWER

National Measurement Laboratory, National Bureau of Standards, Washington, DC 20234, *USA and Laboratory of Molecular Biology, NIAMDD, National Institutes of Health, Bethesda, MD* 20205, *USA*

(*Received* 1 *December* 1980; *accepted* 10 *February* 1981)

Abstract

A technique for improving the precision of crystal data collected on films or with electronic position-sensitive detectors is proposed. The extent of each medium or strong reflection is computed independently, after smoothing and filtering the individual intensities, producing a variable 'dynamic mask'. A method of calculating universal background profiles, which preserves the data and limits the necessary storage, is introduced. The method was applied to data collected with X-ray precession and oscillation techniques and to neutron data collected with a flat-cone diffractometer equipped with a linear detector. In all cases substantial improvement in the precision of weaker reflections was observed. The overall quality of the data was particularly enhanced in the neutron diffraction case.

Introduction

It is quite obvious that the aim of crystallographic data collection should be the measurement of reflection intensities free of systematic errors and with the lowest possible random errors. While it is, in theory, possible (although in practice difficult) to accomplish the former, the latter aim is seldom reached. It can be reached only if we can measure each reflection in such a way that the average error in the results, defined as $\langle\sigma(I)/I\rangle$, will be due only to statistical noise in the measurement of properly defined peaks and backgrounds. In principle, the best way of recording reflections should be to count all X-rays or neutrons scattered during a particular scan through the reflection sphere, isolating exactly those points that belong to the peak from those belonging to the background and summing them accordingly. After that, integrated intensities can be obtained either by profile fitting or, if the spot sizes vary for reflections recorded in different regions of reciprocal space, by normalized subtraction. It should be pointed out, though, that this has not been possible in practice until very recently, when the introduction of position-sensitive area detectors enabled crystallographers to consider three-dimensional scans of reflections. Other techniques used in crystallographic work for recording the reflections can be described as zero-dimensional (stationary single counter or continuously summed scan), one-dimensional (single-counter, step-scan), or two-dimensional (all film methods, linear position-sensitive detectors). All of the latter techniques include some extra background points within the peak area, as will be shown below. In the following discussion we will concentrate on the method which we used to extract optimized data in the two-dimensional cases, but the same approach should be applicable to one- and three-dimensional methods of data collection as well.

The problem of optimizing the signal-to-noise ratio in crystallographic data is of utmost importance to macromolecular crystallographers, who have to measure thousands (or even hundreds of thousands) of reflections from each crystal. Since the total scattering is divided into so many reflections, the intensity of an average reflection is often very little different from the background. The signal-to-noise problem is particularly acute in the collection of neutron scattering data from protein crystals when strong incoherent scattering from hydrogen atoms creates a very high background which can be lowered only by a complete exchange of deuterium for hydrogen.

If the reflections are to be completely recorded in 'zero-dimensional' techniques, the width of the integration area has to be sufficient to allow for experimentally observed movements in actual positions of reflections. Once a reflection has been measured, the only available data are the peak and background intensities. This technique does not allow further improvement in the signal-to-noise ratio, since all information pertaining to reflection shapes and extents has been lost. If any allowance is made for crystal misalignment, then each peak must contain some points actually belonging to the background, and the average error will be higher than the theoretical minimum. If no allowance is made, some peaks may be truncated, introducing systematic error. For these reasons 'zero-dimensional' techniques are not suitable for collection of error-free data with a highly optimized signal-to-noise ratio.

The simplest method of collecting one-dimensional data is by scanning the reflections (for example

employing ω or $\theta/2\theta$ scans) and recording the intensities in a one-dimensional array. A number of methods have been suggested for analyzing reflection profiles in order to obtain improved estimates for the integrated intensities (Slaughter, 1969; Diamond, 1969; Alexander & Smith, 1964). Of particular interest is the method proposed by Lehmann & Larsen (1974). In this technique the ratios of the standard deviations of the integrated intensities to the integrated intensities, $\sigma(I)/I$, are minimized by varying the widths of the Bragg peaks. It is, however, recognized that the method usually underestimates both the integrated intensities and the widths of the peaks (Blessing, Coppens & Becker, 1974; Lehmann, 1975; Grant & Gabe, 1978). The weak reflections are most strongly affected and, if the proper corrections are not made, systematic errors will be introduced into the data. Nevertheless, this method and the others mentioned above lead to better statistical precision for the integrated intensities than the single-peak/background method.

The case of two-dimensional data collection has been represented, until recently, only by various film techniques in which the films were digitized with automatic microdensitometers. Many programming techniques for extracting the integrated intensities of reflections from the digitized image of the film have been proposed, some of them relying on off-line scanning and subsequent processing on a large computer (Abrahamsson, 1969; Xuong, 1969; Werner, 1969; Nockolds & Kretsinger, 1970) and some employing on-line scanning on a minicomputer (Matthews, Klopfenstein & Colman, 1972; Wlodawer, 1974; Sjölin, Olsson & Lindqvist, 1975; see also Arndt & Wonacott, 1977). In most of these techniques a reflection is assumed to reside in a box, with some points along the sides or in the corners of the box used to estimate the background and with the rest assigned to the peak. The conclusion of the International Union of Crystallography Microdensitometer Project (Abrahamsson, Kierkegaard, Andersson, Lindqvist, Lundgren & Sjölin, 1980) was that, even though the statistical errors are not minimized, this approach will suffice in the case of high-quality films. Since it is often necessary to process films which are less than perfect, the quality of data can be substantially improved by the implementation of an approach discussed for one-dimensional data, leading to minimized $\langle\sigma(I)/I\rangle$. Diamond (1969) pointed out that profile fitting techniques will give more precise estimates of the intensities than conventional integration. Ford (1974) has shown that, for two-dimensional data, the underlying assumption of profile fitting techniques is a common shape for all reflections on the film. Spencer & Kossiakoff (1980) have shown that the reflections recorded on a linear position-sensitive detector (this is also a two-dimensional case, with one dimension being the position on the detector and the other the scanning angle) vary much more in size and shape than reflections found on oscillation film, making profile fitting difficult. Therefore, they aimed at finding the extent (but not the height) of every peak by assuming ellipsoidal shapes of reflections and the use of pattern recognition techniques. The improvements noted by Spencer & Kossiakoff for weak neutron data from trypsin were substantial and well justified the introduction of sophisticated methods of data handling. Our work described here was initially directed to improving the quality of data collected from crystals of ribonuclease-A on a flat-cone diffractometer equipped with a position-sensitive linear detector (Prince, Wlodawer & Santoro, 1978; Wlodawer, 1980) and subsequently was extended to other methods of data collection, as will be described below.

Introduction of a universal background estimate

The variance of the net intensity of a reflection is a sum of variances of the peak and of the background. In the case of reflections exceeding the average background level by many times, the variance component, owing to errors in background measurement, will generally be small compared to the variance in the peak, and the gain from improving the estimates of backgrounds will, consequently, be small. In the case of neutron diffraction, however, scattering from many reflections is only a few percent above the background, and thus a poorly determined background can introduce very large errors in integrated intensities, since the integration is accomplished by calculating differences of large and similar numbers. On the other hand, background level is a smooth and slowly varying function in reciprocal space, particularly in the cases of neutron diffraction and of X-ray data obtained with the help of a monochromator, where streaks caused by white radiation are not present. Thus a procedure for calculating average backgrounds based on many reflections was shown by Spencer & Kossiakoff (1980) to improve significantly the quality of neutron data collected from a small trypsin crystal. The procedure we propose is similar but has two important differences. Firstly, the background described by Spencer & Kossiakoff (1980) for their system of three linear detectors was considered as a function of the position on the detector but not of the angle of rotation of the crystal, Ψ. Since we could not fully justify this assumption, we have also described the background as a slowly varying function of Ψ. Secondly, for reasons of limited available computer storage, most data aquisition systems in general use do not save a large proportion of the background data but calculate the background values from points within each reflection box only. The loss incurred in this procedure can be shown in the following example. Let us consider a very weak reflection with the intensity barely exceeding the

background level. In a typical data collection for ribonuclease-A about half of the points are assigned to the boxes containing the reflections and half are background only, and most procedures reject the latter half of the data. Since about half of the points within each box are found to belong to a peak and another half to the background, the variance for the integrated intensity would be

$$\mathrm{var}(I) \simeq \sum^{p} I(i) + \mathrm{var}\left[\sum^{p} B(i)\right], \qquad (1)$$

where the summation is over the p points in the peak and $B(i)$, the background, is a function derived from the remaining b points (Lehmann & Larsen, 1974). It can also be shown that

$$\mathrm{var}\left[\sum^{p} B(i)\right] = \frac{p^2}{b}\bar{B}, \qquad (2)$$

where $\bar{B}$ is the average background value. By including all possible background points in the calculation, their number is increased about threefold; and, subsequently, the ratio of the background component of the variances for the two cases will decrease by a factor of three if all available background points are included in the calculations.

Since the lack of computer storage capacity precluded direct saving of all background points, the following procedure was implemented. Each frame of data was checked, and all data belonging to reflection boxes were removed and stored on the disk. Remaining points were used to update a 'universal background' array computed in a manner suggested by Xuong, Freer, Hamlin, Nielsen & Vernon (1978). Each universal background point along the detector was recalculated by adding a suitable fraction of the new value (usually $f = \frac{1}{16}$) to the old value multiplied by $(1 - f)$, and the values for the missing points were obtained by interpolation. When a complete reflection was collected, a polynomial was fitted, by least squares, to the part of the universal background in the vicinity of the reflection (usually 50 channels each way), and the resulting coefficients were stored together with the reflection (*cf.* Figs. 1 and 2). This procedure reduces the amount of background data from several hundred numbers to only three or four per reflection while preserving the information content. Estimated background is available for each reflection even before the data within each reflection box are considered, and this proves to be very useful in detecting the shapes, sizes, and positions of the peaks, as will be described below.

Dynamic mask procedure

This procedure is designed to calculate the position and extent of a reflection peak in a box also containing background points with considerable noise. It is equally applicable to one-, two-, and three-dimensional data, but in what follows we will concentrate on the two-dimensional case, since extension of the method is relatively straightforward.

Let us assume that a particular reflection is completely enclosed within a box and that no other

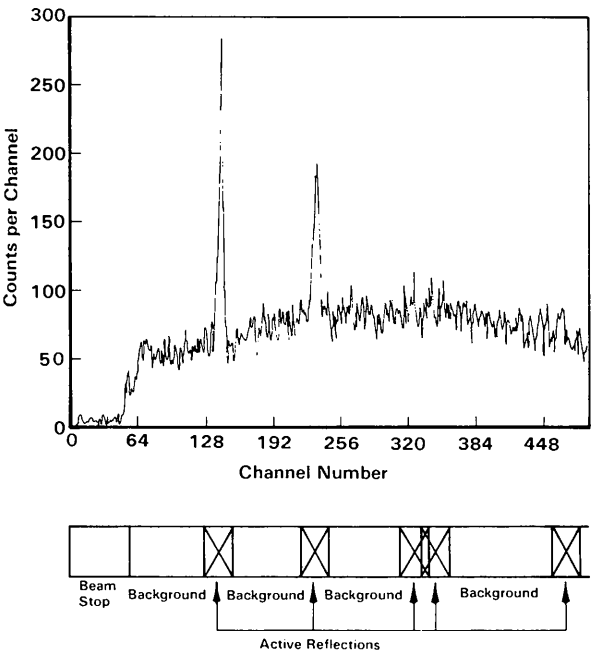

Fig. 1. An example of a frame of data collected with a linear position-sensitive detector. The areas attributed to reflections, background and the beam-stop shadow are marked below.

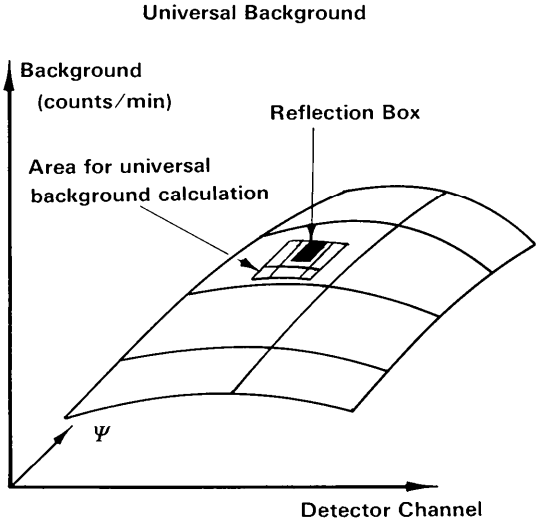

Fig. 2. A schematic diagram showing the areas used to calculate the universal background in the vicinity of a reflection. The background is described as a slowly varying function of the position on the detector and of the crystal rotation angle Ψ.

reflections are intruding into the background. Since the noise level is high (see Fig. 3), any point within the box may be found to be above the average background level, but only the points belonging to the actual reflection are expected to be contiguous. Random noise can be suppressed by smoothing the data and by including at each point some contribution from its neighbors. We have chosen a generalized version of the formula used by Spencer & Kossiakoff (1980):

$$I_{i,j} = [A\,(I_{i-1,j-1} + I_{i-1,j+1} + I_{i+1,j-1} + I_{i+1,j+1}) + B(I_{i,j-1} + I_{i,j+1} + I_{i-1,j} + I_{i+1,j}) + CI_{i,j}]/(4A + 4B + C). \quad (3)$$

Initially we did not restrict the values of A, B, and C but experimented with varying these parameters. The best values found for very noisy data were $A = 1$, $B = 2$, and $C = 3$. For less-noisy data, decreased contributions from the neighbors gave better results. The effect of the smoothing procedure can be seen in Fig. 3. The parameters need to be chosen for each system in such a way that the peak boundary will not be widened more than necessary.

Once the data have been smoothed, it is possible to apply a 'statistical filter' (Ford, 1974; Kabsch, 1977; Rossmann, 1979) to distinguish between the data belonging to the peak and to the background. These procedures were modified in the neutron case to include the initial estimate of the background from the 'universal background' data. Once the background level and its variance have been established, either directly, on the basis of the points unlikely to contain peak information, or on the basis of the universal background, the background is subtracted from each point and a flag is set, depending on whether the net intensity exceeds the background by less than σ (0), between σ and 2σ (1), 2σ and 3σ (2), over 3σ (3). The so called 'sigma array' corresponding to the reflection shown in Fig. 3 can be seen in Table 1. It is quite evident that the peak is contiguous, while the noise in

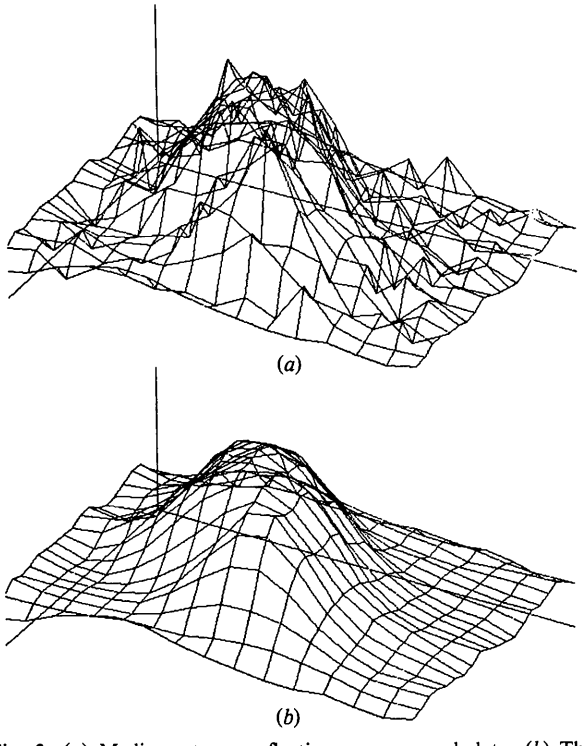

Fig. 3. (*a*) Medium strong reflection, unprocessed data. (*b*) The same data after application of a nine-point parabolic smoothing procedure.

Table 1. *The dynamic mask procedure applied to a well resolved reflection*

Detector output

151	121	92	78	78	75	81	69	80	90	95	88	85	81	81	92	79	72	83
94	103	81	82	84	89	98	85	87	86	98	82	85	103	103	82	96	64	78
90	85	87	102	86	96	79	98	75	102	97	82	82	100	84	83	85	77	94
90	78	93	80	85	80	87	101	78	84	71	81	74	100	81	77	87	83	82
89	66	82	72	79	95	93	80	72	81	89	79	83	99	95	87	85	69	90
100	75	80	88	73	100	89	101	83	87	76	79	79	84	92	92	74	96	82
83	100	81	87	82	106	90	88	68	98	82	76	83	110	96	82	87	75	90
75	83	91	80	92	93	93	90	86	85	80	81	87	84	83	89	82	86	85
79	98	114	82	86	88	84	91	87	77	90	86	89	86	90	84	80	113	96
99	77	86	80	104	93	80	83	73	88	102	76	91	96	124	89	95	72	77
80	98	80	82	98	87	72	107	81	96	87	100	117	123	103	89	115	83	85
84	74	77	78	96	89	83	65	95	89	104	120	135	160	127	93	79	90	77
89	80	84	79	85	96	96	78	88	104	133	163	169	154	117	88	95	103	86
78	92	93	95	85	90	98	90	115	116	158	206	191	122	89	84	88	101	80
96	78	82	84	84	82	112	112	152	169	200	204	173	100	82	82	74	85	91
104	95	93	90	83	105	127	165	162	219	184	166	110	83	82	104	84	86	85
97	79	96	99	101	130	142	173	215	205	143	141	103	82	78	89	75	79	78
80	92	104	91	126	168	190	194	198	161	109	99	104	91	88	76	96	87	104
106	76	82	104	141	198	233	186	176	93	84	83	91	80	91	96	98	97	105
92	83	97	117	196	200	197	152	125	100	96	84	92	97	91	88	99	87	91
72	90	118	150	148	173	138	98	90	85	80	64	90	93	97	105	84	110	82
79	108	102	149	166	131	98	83	90	88	90	100	90	103	88	78	97	100	83
72	94	104	127	111	92	99	113	93	94	86	93	85	101	106	101	99	84	77
81	93	101	105	103	101	99	82	94	79	93	101	93	90	88	95	95	101	85
66	86	111	101	79	91	97	88	77	82	93	95	87	96	98	92	113	118	106
103	94	94	85	84	84	87	97	100	86	95	103	102	102	96	90	94	93	102
93	89	86	103	88	101	83	93	95	103	90	76	111	81	110	87	96	81	96
80	75	84	83	88	86	64	105	81	83	77	94	88	83	95	101	109	98	115
101	97	98	89	95	78	90	106	91	84	91	105	93	86	101	86	108	118	140
104	105	94	88	103	75	102	96	99	82	85	102	64	96	106	134	128	146	168
91	97	98	104	91	94	111	83	98	96	78	97	110	99	137	140	157	179	171

Sigma array	Final mask
0 0 0 0 0 0 0 0 0 0 0 0 0 0 0 0 0 0 0 0 0	0 0 0 0 0 0 0 0 0 0 0 0 0 0 0 0 0 0 0 0 0
0 0 0 0 0 0 0 0 0 0 0 0 0 1 0 0 0 0 0	0 0 0 0 0 0 0 0 0 0 0 0 0 0 0 0 0 0 0 0 0
0 0 0 0 0 1 0 1 0 0 0 0 0 0 0 0 0 0 0	0 0 0 0 0 0 0 0 0 0 0 0 0 0 0 0 0 0 0 0 0
0 0 0 0 0 1 0 0 0 0 0 0 0 1 1 0 0 0 0	0 0 0 0 0 0 0 0 0 0 0 0 0 0 0 0 0 0 0 0 0
0 0 0 0 0 1 0 0 0 0 0 0 0 0 0 0 0 0 0	0 0 0 0 0 0 0 0 0 0 0 0 0 0 0 0 0 0 0 0 0
0 0 2 0 0 0 0 0 0 0 0 0 0 0 0 0 1 0	0 0 0 0 0 0 0 0 0 0 0 0 0 0 0 0 0 0 0 0 0
0 0 0 0 1 0 0 0 0 0 0 0 2 2 0 0 0 0	0 0 0 0 0 0 0 0 0 0 0 0 0 1 1 0 0 0 0
0 0 0 0 1 0 0 0 0 0 1 1 3 3 3 0 1 0 0	0 0 0 0 0 0 0 0 0 0 0 0 1 1 1 1 1 0 0 0 0
0 0 0 0 0 0 0 0 0 1 1 3 3 3 3 0 0 0 0	0 0 0 0 0 0 0 0 0 0 0 1 1 1 1 1 1 0 0 0 0
0 0 0 0 0 0 1 0 1 1 3 3 3 3 3 0 0 2 0	0 0 0 0 0 0 0 0 0 0 1 1 1 1 1 1 1 0 0 0 0
0 0 0 0 0 0 1 0 3 3 3 3 3 3 0 0 0 1 0	0 0 0 0 0 0 0 0 0 1 1 1 1 1 1 1 0 0 0 0 0
0 0 0 0 0 0 2 3 3 3 3 3 3 2 0 0 0 0 0	0 0 0 0 0 0 1 1 1 1 1 1 1 1 1 0 0 0 0 0
1 0 0 0 0 2 3 3 3 3 3 3 3 0 0 1 0 0 0	0 0 0 0 0 1 1 1 1 1 1 1 1 1 1 0 0 0 0 0
0 0 1 0 2 3 3 3 3 3 3 3 2 0 0 0 0 0 0	0 0 0 0 1 1 1 1 1 1 1 1 1 1 0 0 0 0 0 0
0 0 1 1 3 3 3 3 3 3 2 2 1 0 0 0 0 0 1	0 0 1 1 1 1 1 1 1 1 1 1 1 0 0 0 0 0 0 0
1 0 0 1 3 3 3 3 3 2 0 0 0 0 0 0 2 0 1	0 0 0 1 1 1 1 1 1 1 1 0 0 0 0 0 0 0 0 0
0 0 1 3 3 3 3 3 3 1 0 0 1 0 0 1 0 1 0	0 0 1 1 1 1 1 1 1 1 0 0 0 0 0 0 0 0 0 0
0 0 3 3 3 3 3 1 0 0 0 0 0 1 1 0 1 1 0	0 0 1 1 1 1 1 1 0 0 0 0 0 0 0 0 0 0 0 0
0 1 3 3 3 3 1 0 0 0 0 0 1 1 0 0 0 1 0	0 0 1 1 1 1 1 0 0 0 0 0 0 0 0 0 0 0 0 0
0 1 1 3 3 1 1 1 1 0 0 0 0 1 1 1 1 0 0	0 0 1 1 1 1 1 1 0 0 0 0 0 0 0 0 0 0 0 0
0 0 1 2 1 1 1 0 0 0 0 1 0 0 0 0 1 1 0	0 0 1 1 1 1 1 1 0 0 0 0 0 0 0 0 0 0 0 0
0 0 2 1 0 0 0 0 0 0 0 1 0 1 1 1 2 3 1	0 0 1 1 0 0 0 0 0 0 0 0 0 0 0 0 0 0 0 0
0 1 0 0 0 0 0 1 0 0 1 1 2 1 1 0 1 0 1	0 0 0 0 0 0 0 0 0 0 0 0 0 0 0 0 0 0 0 0
0 0 0 0 1 1 0 1 1 1 0 0 1 0 1 0 0 0 1	0 0 0 0 0 0 0 0 0 0 0 0 0 0 0 0 0 0 0 0
0 0 0 0 0 0 0 0 0 0 0 0 0 0 0 1 2 2 2	0 0 0 0 0 0 0 0 0 0 0 0 0 0 0 0 0 0 0 0

Reflection index 2 − 2 −10.
Intensity with applied mask = 4871·87.
Estimated sigma 129·17 I/SIGMA = 37·72

the background is random. We can now create a mask for this reflection from the contiguous part of the 'sigma array' including all points flagged 1, 2, or 3. We call this mask 'dynamic', since it is calculated independently for each medium or strong reflection and its shape, size, and position of the center are not constrained.

Integrated intensities are now calculated from the original data array by summing all elements covered by the mask and subtracting their background. We should stress that the smoothed data are used only in constructing the mask. They are not, as in some peak fitting techniques, used in actual integration. The variance of the integrated intensity is calculated from counting statistics, with a formula derived by Lehmann & Larsen (1974) assuming Poisson distribution for the $I(i)$,

$$\sigma^2(I) \simeq \sum^{p} \text{var}\, I(i) + \sum^{p} \text{var}[B(i)], \qquad (4)$$

where $I(i)$ and $B(i)$ are the points belonging, respectively, to the peak and background. To check if the assumption of Poisson distribution holds, we also calculate purely statistical variance according to Phearson (1975),

$$\sigma^2(I) = \sigma^2(B)\left[N_i + \frac{N_i^2}{N_b} + \text{co}\ \sigma^2(I)\right], \qquad (5)$$

where $\sigma^2(B)$ is the variance in background, N_i and N_b are the numbers of elements in the peak and background, and co $\sigma^2(I)$ is a covariance term, normally equal to zero. It is always included as a tool for checking errors not likely to be found without visual examination of all reflections.

The procedure described here will not provide accurate estimates of intensity for weaker reflections [$I < 10\sigma(I)$] which may not create a contiguous mask. In this case we apply a mask calculated for a neighboring medium or strong reflection, including the position of its center of gravity. In this way we can avoid biasing weaker reflections for which the intensities contained in the elements $\sigma = 0$ of the sigma array could make a substantial contribution to the integrated intensity. For this purpose we store a number of masks corresponding to different areas on the detector and reciprocal space and update them throughout data processing. If a weak reflection is measured before any actual masks are calculated, we can use a starting mask precalculated on the basis of previous experience. This small departure from generality is unlikely to introduce serious errors.

Treatment of reflection boxes containing contributions from more than one reflection

The procedure used to calculate a dynamic mask made the assumption that the box under consideration contains only one reflection. This is not always the case, and while the presence of other reflections can be predicted from the orientation matrix of the crystal, such calculations may be cumbersome in practice, especially for geometries such as normal beam (rotation photography) or flat cone (used in our neutron studies). On the other hand, comparison of universal and local background can quickly alert us to such a possibility, since, if parts of other reflections are present in the area from which local background is computed, its value will be higher than that for universal background. In the case when universal background has not been calculated, it is possible to detect intruding reflections on the basis of the statistical distribution of background intensities.

When a putative mask has been constructed for a particular reflection, the areas belonging to the local

The Dynamic Mask Algorithm

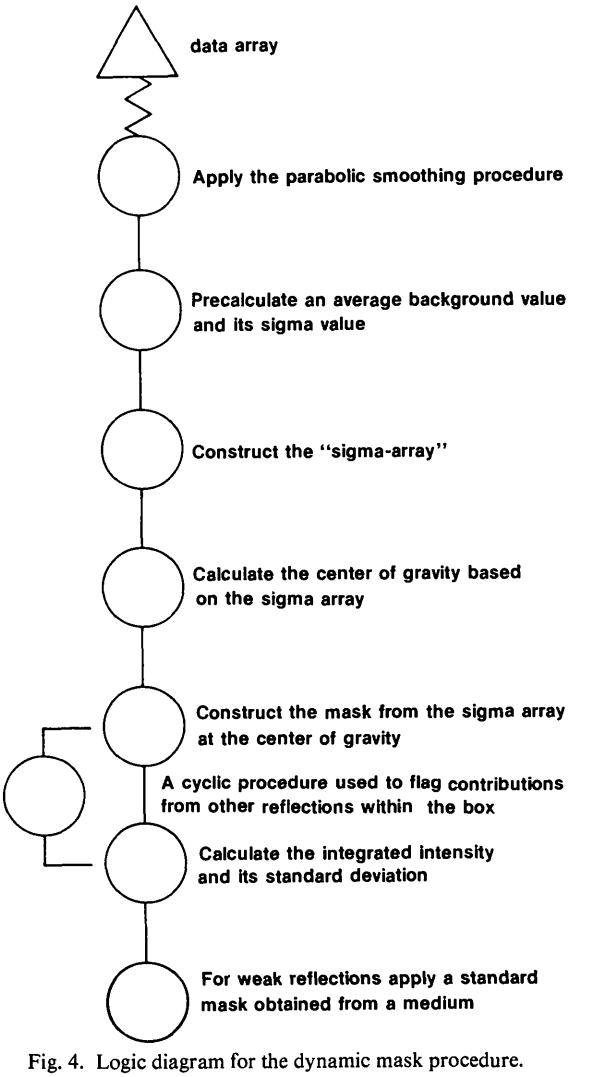

Fig. 4. Logic diagram for the dynamic mask procedure.

background are analyzed with a cyclic procedure (see Fig. 4). We make the assumption that, if the background elements contain only random noise, their intensities will be distributed around a true average value and have a normal distribution. In such a case removing the elements which deviate from the average by more than, say, three standard deviations should not change the average value. If, however, some of the intensities are affected by another reflection, their rejection will lower the average intensity of the background. The points falling outside the limits of the normal distribution are flagged and are not used further. A new average and variance are calculated on the basis of the remaining background points. These calculations quickly converge, and we find that stable values of the background are available after three cycles at most. It is also clear that this procedure usually increases the number of points attributed to the background compared to the initial estimate and, in general, prevents serious underestimation of the peak intensity.

A reflection box containing a weak reflection in the presence of two much stronger neighboring reflections is seen in Table 2. The dynamic mask shown clearly distinguishes between the peak and the background areas, but since the reflections are very close, it does not directly distinguish the central reflection from its neighbors. However, this might be treated more properly by restraints on the size of the mask, which is included in our version for oscillation film data, or reflections can be separated on the basis of the known extent of the peaks or alternatively by considering the projections of the integrated intensities.

Table 2. *A box containing a weak reflection in the presence of two much stronger reflections*

Points marked −1 were considered on the basis of the normal distribution of background intensities to belong to the other reflections and were not used for integration.

Detector output

72	60	62	71	60	76	72	71	71	76	70	74	85	116	152	259	293	381	438
77	86	64	94	68	73	71	73	71	65	67	66	95	119	240	344	399	410	441
62	97	74	67	91	77	44	69	80	67	60	66	99	192	300	425	489	441	302
64	54	62	75	71	60	80	78	75	57	74	65	123	211	462	431	391	290	157
56	70	79	79	68	60	72	66	69	72	80	83	156	291	431	386	259	154	131
81	84	77	69	69	71	66	72	53	68	85	104	149	334	360	263	142	119	72
66	82	72	71	84	69	72	69	64	74	63	91	159	296	244	156	87	81	76
66	70	63	91	76	56	81	81	68	77	69	78	162	190	151	97	91	76	63
75	60	70	106	85	58	64	59	95	73	76	91	129	119	81	81	70	78	67
60	71	66	74	70	69	61	84	75	66	80	84	91	84	68	70	77	68	76
64	64	89	61	75	72	66	81	60	77	68	93	79	70	76	66	85	69	70
77	65	70	74	70	58	78	63	90	64	81	93	74	85	63	84	72	60	70
68	92	62	66	77	73	68	67	70	75	74	65	84	91	60	66	56	68	74
92	73	59	81	62	70	69	74	66	89	74	88	73	74	75	80	58	84	70
62	68	78	69	75	78	81	74	57	81	90	85	59	79	71	77	74	81	81
75	64	75	80	72	67	64	77	84	87	63	88	65	77	78	68	73	81	62
60	69	60	71	74	82	83	79	70	69	87	82	69	67	54	63	64	61	60
72	81	62	75	88	86	91	71	82	83	85	59	75	76	60	76	75	86	57
76	61	63	77	75	86	96	74	84	72	68	58	65	67	61	84	89	70	88
88	56	83	81	77	85	92	79	80	78	87	73	86	67	84	83	59	57	75
70	78	80	84	74	81	81	87	93	76	76	75	65	84	71	63	82	58	74
65	82	57	74	84	94	85	69	78	70	84	74	67	78	83	86	61	71	84
75	73	60	80	89	85	76	76	64	75	62	65	73	81	60	65	72	69	70
72	67	88	86	80	73	74	65	84	72	70	73	62	83	70	76	79	76	92
78	73	77	78	82	71	69	82	83	82	93	83	69	70	72	83	66	77	73
80	96	92	92	67	67	79	78	72	78	75	80	73	92	66	87	66	85	73
81	82	98	90	71	80	83	67	79	67	72	76	50	75	68	72	73	64	77
93	102	105	93	67	86	77	69	71	82	69	62	76	74	73	90	94	83	82
122	136	109	82	73	77	69	84	87	78	69	78	82	90	81	70	72	78	63
146	144	149	82	82	80	71	74	64	73	66	67	82	64	93	95	77	72	85
209	203	143	88	81	75	70	80	85	60	86	69	67	68	66	76	69	73	77

Final mask

−1	−1	0	0	0	0	0	0	0	0	0	0	−1	−1	−1	−1	−1	−1	−1
0	0	0	0	0	0	0	0	0	0	0	−1	−1	−1	−1	−1	−1	−1	−1
0	0	0	0	0	0	0	0	0	0	0	−1	−1	−1	−1	−1	−1	−1	−1
0	0	0	0	0	0	0	0	0	0	0	−1	−1	−1	−1	−1	−1	−1	0
0	0	0	0	0	0	0	0	0	0	0	−1	−1	−1	−1	−1	−1	0	0
0	0	0	−1	0	0	0	0	0	0	0	−1	−1	1	−1	0	0	0	0
0	0	0	0	0	0	0	0	0	0	0	1	1	1	0	0	0	0	0
0	0	0	0	0	0	0	0	0	0	1	1	1	1	0	0	0	0	0
0	0	0	0	0	0	0	0	0	1	1	1	1	1	1	0	0	0	0
0	0	0	0	0	0	0	0	1	1	1	1	1	1	1	0	0	0	0
0	0	0	0	0	0	0	1	1	1	1	1	1	1	1	0	0	0	0
0	0	0	0	0	1	1	1	1	1	1	1	1	1	1	0	0	0	0
0	0	0	0	1	1	1	1	1	1	1	1	1	1	1	0	0	0	0
0	0	0	1	1	1	1	1	1	1	1	1	1	1	0	0	0	0	−1
0	0	1	1	1	1	1	1	1	1	1	1	1	1	0	0	0	0	0
0	0	1	1	1	1	1	1	1	1	1	1	1	0	0	0	0	0	0
0	0	1	1	1	1	1	1	1	1	1	1	0	0	0	0	0	0	0
0	1	1	1	1	1	1	1	1	1	1	0	0	0	0	0	0	0	0
0	1	1	1	1	1	1	1	1	1	0	0	0	0	0	0	0	0	0
0	1	1	1	1	1	1	1	1	0	0	0	0	0	0	0	0	0	0
0	1	1	1	1	1	1	1	0	0	0	0	0	0	0	0	0	0	0
0	1	1	1	1	1	1	0	0	0	0	0	0	0	0	0	0	0	0
0	1	1	1	1	1	0	0	0	0	0	0	0	0	0	0	0	0	0
0	1	1	1	1	0	0	0	0	0	0	0	0	0	0	0	0	0	0
−1	−1	−1	−1	0	0	0	0	0	0	0	0	0	0	0	0	0	0	0

Applications

The dynamic mask procedure has been applied to three different techniques of data collection. In two of them (flat-cone neutron diffractometer equipped with a linear position-sensitive detector and X-ray oscillation photography), the predicted positions of the peaks within their boxes are subject to errors, owing to the uncertainty of the orientation matrices, crystal movement, drifts in electronic components, *etc.* X-ray precession photography differs from the other two methods in that the peak positions are better known and their profiles are more uniform. Since the requirements of these techniques differ widely, the applications will be discussed separately. All calculations were run on a virtual memory VAX11/780 computer, with an average data processing speed of two reflections s^{-1}.

Neutron data collected with a linear position-sensitive detector

The dynamic mask procedure was originally developed to improve the data collected with the National Bureau of Standards flat-cone diffractometer. The algorithm was extensively tested during data collection on a large (30 mm^3) crystal of ribonuclease-A. The details of sample preparation and treatment were given by Wlodawer (1980), and the diffractometer hardware and programs were described by Prince *et al.* (1978). The main difficulties in collecting useful neutron data as summarized by Spencer & Kossiakoff (1980) apply equally to this study. The principal difficulty arises from the incoherent inelastic scattering of hydrogen atoms present in the sample. Even though the crystal under study has been

deuterated by slow solvent exchange for a period of over six months prior to the onset of data collection, it can be estimated that well over 25% of the protein atoms in the crystal (and over 10% of all the atoms in the sample and mounting) are hydrogens, and consequently high background level is unavoidable. Another problem was caused by the drifts in the diffractometer electronics, which would cause changes in the relationship between the reflection positions in the laboratory coordinate system and the channel number in the detector [the diffractometers used in this study and by Spencer & Kossiakoff (1980) had similar detectors and electronics]. As a result, data integrated using the algorithm of Prince *et al.* (1978) (calculating fractional indices corresponding to each point on the detector and summing those in the vicinity of a reciprocal-lattice point) suffered from a poor signal-to-noise ratio, and a new approach was indicated.

The dynamic mask procedure was tested in a way similar to that used by Spencer & Kossiakoff (1980). The data for each peak were contained in a 19 × 31 box, and the integrated intensities were calculated by summation of a smaller array (15 × 25 points) centered within the box, taking the remainder as the background. The integrated intensity was calculated as $I = P - (N_i\ B)/N_b$, where N_i and N_b are the numbers of points in peak and background, respectively. The variances for integrated intensities were calculated directly on the basis of this formula (see equation 1). If we assume that a reflection is 'observed' if its intensity exceeds its σ by a predetermined factor (in our case, 3), the number of observed reflections found with the help of the dynamic mask algorithm should exceed the number indicated by the standard box procedure, owing to better statistics. Fig. 5 shows that this assumption was justified. As an example, the 0*kl* level contains 1427 theoretically accessible reflections to 2 Å resolution. Of that number standard box procedure found that 937 had significant intensities, while the dynamic mask procedure indicated 1168 observed reflections.

An indication of the quality of the data produced by both procedures was obtained by investigation of symmetry agreement factors defined as

$$R_{\rm sym} = \frac{\sum_i |I_i - \bar{I}|}{\sum I_i} \times 100\% \qquad (6)$$

for each of the data sets. It should be stressed that the absolute value of $R_{\rm sym}$ is not a good indication of the relative quality of two different data sets, since this indication is strongly affected by phenomena such as absorption and extinction; but in our case we were comparing two sets of estimates of the same intensities, identically influenced by systematic errors. In the example above, $R_{\rm sym}$ became 6·7% for the standard technique and 4·9% for the dynamic mask procedure (Table 3). The relationship between average intensities and $R_{\rm sym}$ are plotted in Fig. 6, clearly showing that the dynamic mask procedure is most beneficial for weaker reflections. Table 3 also contains the values of $R_{\rm sym}$ calculated on structure amplitudes corrected for absorption (Santoro & Wlodawer, 1980) and for the

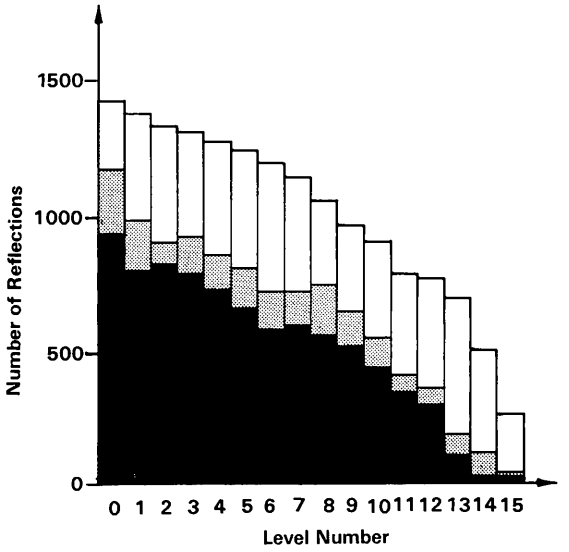

Fig. 5. A histogram of the total number of reflections collected during a 360° rotation of a ribonuclease crystal with a position-sensitive detector for the levels *nkl*. Black reflections observed with a box procedure; shadowed extra observed reflections found by the dynamic mask procedure; white unobserved reflections.

Table 3. *R_{sym} values calculated according to equation (6) for each level in 2·0 Å neutron data for ribonuclease-A and given for both a standard box procedure and the dynamic mask algorithm*

Level number	$R_{\rm sym}$ (%) Standard box	Dynamic mask
0	6·7	4·9
1	7·1	5·3
2	6·9	5·4
3	7·6	5·8
4	7·5	4·6
5	8·1	6·0
6	7·8	5·1
7	7·9	5·7
8	8·6	5·5
9	8·8	7·0
10	9·1	6·4
11	8·6	6·2
12	10·2	7·2
13	10·6	8·0
14	12·6*	8·2*
15	–	9·9*

* Not a significant number of symmetry mates in the level (less than 15).

effects of parallax, Lorentz correction, *etc.* Again, the superiority of the dynamic mask procedure is obvious. It might be interesting to point out that the values of R_{sym} calculated on F's were slightly larger than those calculated on raw intensities. This can be explained by noting that $I \sim F^2L$, where, for flat-cone and equatorial geometries (but not for precession geometry), the Lorentz factor L is a monotonically decreasing function of resolution. Since the average intensities are also decreasing as a function of resolution, there is a positive correlation between L and I. Thus R_{sym} defined in (6) is dominated by the well-determined low-angle measurements, while high-resolution data determines the value of R_{sym} calculated on the basis of F's. This again points out that absolute values of R_{sym} calculated on intensities should not be used for comparison of the data from different experiments but might be used as a measure of the accuracy of different procedures applied to the same test data set.

A better estimate of the absolute quality of the data can be obtained by comparison of the reproducibility in repeated experiments. Data for one of the levels (7*kl*) have been collected several times and processed with the dynamic mask procedure, and the resulting indicators, R_{rep}, defined as

$$R_{rep} = \frac{\sum_i |I_i - \bar{I}|}{\sum I_i} \times 100\% \qquad (7)$$

were compared (Table 4). This indicator sets the lower level on the accuracy of the methods, with other errors decreasing the expected quality of the data. This experiment also provided us with the capability to estimate statistical standard deviations of the intensities,

$$\sigma_s = \left[\frac{\sum_n (I_i - \bar{I})^2}{n-1}\right]^{1/2}, \qquad (8)$$

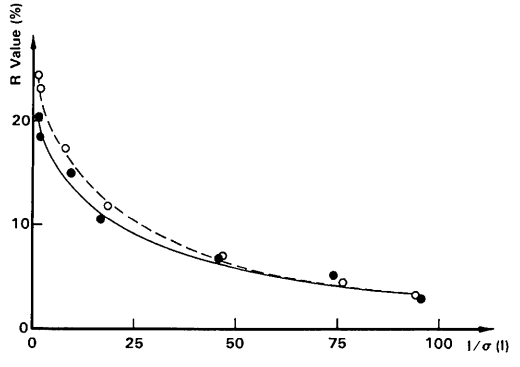

Fig. 6. Symmetry R factors plotted as a function of $\sigma(I)/I$ for the intensities obtained with a box procedure (○) and the dynamic mask procedure (●). Ribonuclease, level 7*kl*.

Table 4. *Result of an intensity interval analysis of R values, measured and calculated* $\langle\sigma/I\rangle$, *obtained from reproducibility measurements of the level 7kl for a ribonuclease-A crystal*

Interval number	Average intensity	Number of reflections	R value (%)	Measured $\langle\sigma/I\rangle$ (%)	Calculated $\langle\sigma/I\rangle$ (%)
1	563	74	32·0	26·8	45·3
2	710	192	19·7	20·3	27·9
3	1195	168	14·0	10·3	19·8
4	2706	174	9·8	4·8	13·9
5	6029	60	5·8	2·8	8·2
6	16411	62	4·3	1·4	6·1
Total		730	6·5	6·9	9·2

and to compare them with the estimates of the standard deviation based on the variances within the data in reflection boxes (*cf.* Table 4).

Another measure of the precision of the data collected with flat-cone geometry was obtained by the comparison with the structure amplitudes collected to the resolution of 2·8 Å on the same instrument but with a different crystal and equatorial geometry of the diffractometer (Wlodawer, 1980). The structure amplitudes were scaled with the procedure of Hamilton, Rollett & Sparks (1965), and again we can see that the agreement is better between the dynamic mask data and the equatorial data than between the standard box and the equatorial data (Table 5). Finally, 2 Å data were used in successful refinement of the structure of ribonuclease (Wlodawer & Sjölin, 1981).

Film data

Film techniques still retain their importance for protein data collection in many laboratories. While precession methods are particularly useful in the search for heavy-atom derivatives, oscillation photography has become, in the last few years, a principal method of collecting data from crystals with large unit cells. Ford (1974) has previously shown that an algorithm capable of distinguishing between peak and background can provide better estimates of integrated intensities in precession photography. Similar results were obtained by Kabsch (1977) and Rossmann (1979) for the oscillation method. For these reasons, we have implemented the dynamic mask procedure in the existing computer programs for processing of precession and oscillation films and compared the results with those obtained with the standard box procedure.

The first system used to test the precession software consisted of 19° photographs of ribonuclease-A, taken on a new, very-low-background film, CEA Reflex 25. These films were of excellent quality with low and uniform background (average OD = 0·16, for details see Abrahamsson, Lindqvist, Sjölin & Wlodawer, 1981) and uniform spot shapes, and with almost all reflections observed. The films were scanned off-line on

Table 5. *Scaling of structure amplitudes calculated from intensities obtained with (a) standard box; (b) dynamic mask procedures against (c) structure amplitudes measured with the position-sensitive linear detector operating in equatorial geometry*

R_{sca} is given according to $R_{sca} = \frac{\sum |F_1 - sF_2|}{\sum F_1} \times 100\%$

for each level.

Level number	R_{sca} (%)		
	(a)/(b)	(a)/(c)	(b)/(c)
0	6·3	6·9	5·5
1	6·8	7·2	5·8
2	6·5	7·6	6·2
3	7·3	8·3	7·0
4	7·4	7·5	6·7
5	7·6	7·6	6·4
6	7·2	8·3	6·8
7	8·4	8·8	6·9
8	8·4	8·7	7·1
9	8·9	10·1*	9·8*
10	9·7	–	–
11	9·2	–	–
12	10·4	–	–
13	10·6	–	–
14	13·7*	–	–
15	–	–	–

* Not significant since less than 15 reflections appeared in both data sets.

an Optronics P-1000 film scanner, and the integrated intensities were calculated within identical boxes by a standard procedure and by the dynamic mask procedure. In the latter case we did not calculate the universal background, relying only on the background estimates in the immediate vicinity of each peak. To compare the results, values of R_{sym} for four sets of symmetry-equivalent reflections present on each film were calculated for each method according to (6). For a typical ribonuclease film, R_{sym} = 3·9% for the standard box procedure and 3·7% for the dynamic mask procedure. When the values of R_{sym} were calculated in intervals of integrated intensity, they were identical for stronger reflections, while the dynamic mask procedure produced slightly better results for the weak ones. This result is not surprising and it shows that the procedure is most useful in those cases when the data are noisy and weak. It also points out that the value of R_{sym} is so influenced by strong reflections that significant improvements in the estimates of weaker reflections will not show properly without considering the distribution of R's (*cf.* Abrahamsson *et al.*, 1980).

Another set of precession photographs used in the tests of the method was collected on crystals of *Rhisopus chinensis* acid protease by Dr R. Bott. These photographs were characterized by poor resolution of reflections along the shortest reciprocal axis. For a typical film we found R_{sym} = 8·0% for the standard box procedure and 5·0% for the dynamic mask procedure. Visual inspection of the films and of the scanner outputs showed that the principal effect responsible for this considerable improvement was the capability of the dynamic mask procedure to remove the influence of the neighboring reflections and, hence, to allow all other points in the box to be separated into peak and background areas for the final calculation of integrated intensities.

While precession photographs offer less challenge in their processing, owing to the regularity of the patterns and the ease of prediction of spot locations, this is not true for oscillation photographs. Indeed, most methods attempting to improve the quality of scanner data are being developed for this technique. In our tests we were provided with a set of oscillation programs written by Cornick & Navia (1980), and we used photographs taken by Dr M. Navia during his collection of a 2·5 Å native data set on an immunoglobulin J539. Again, for integration we used the same reflection boxes as in the standard box procedure, and we did not use the universal background. For all the films the improvement in R_{sym} was substantial. For one film, R_{sym} was lowered from 6·6 to 3·7% and for another, weaker film from 9·3 to 6·7%. Table 6 shows the printout of a typical reflection sandwiched between two close neighbors, and it emphasizes why good definition of the peak and background areas is crucial to improving the quality of data from such films.

Discussion

The dynamic mask procedure has now been tested with three different two-dimensional techniques of data collection. The results show quite convincingly that, in most cases, one can expect substantial improvement in data quality, unless exceptionally well diffracting crystals and low-background films are used. Even in that case, improvement in the estimates of weaker reflections was observed. In the X-ray techniques the limits in the data quality came mostly from reflection overlap and the necessity to include extra points in the peak or intruding into the predefined background area, thus lowering the statistical precision of the data. In the neutron scattering case, the most important difficulty lies in very low peak-to-background ratios, and in that case calculation of the universal background can substantially improve the final estimates of integrated intensities.

Even though all the tests of the method were performed with two-dimensional data, there is nothing in the algorithm which would prevent its use in either a one-dimensional or a three-dimensional case. This differs from techniques such as the ellipse fitting procedure of Spencer & Kossiakoff (1980), which is not easily extended to three dimensions, owing to an excessive number of required parameters. Indeed, in the programs written for a diffractometer equipped with an

Table 6. *A reflection measured on an X-ray oscillation film of an immunoglobulin* J539

The areas used for standard box integration are marked. For the box procedure the average background is 91·8 and the net intensity 914, while for the dynamic mask procedure they are 86·5 and 1139 respectively.

Background area 1						Peak area											Background area 3					
83	85	85	81	83	84	81	83	83	85	85	83	85	82	83	86	87	90	89	87	85	91	87
85	85	83	83	81	83	85	81	87	87	84	84	85	87	85	87	87	89	90	87	89	94	95
87	85	89	89	85	83	85	83	85	85	85	87	89	85	86	87	90	83	89	94	98	107	109
87	89	91	90	85	85	89	87	88	86	89	94	96	87	87	88	91	89	94	107	129	134	135
98	113	113	107	98	94	91	88	87	98	116	116	116	107	98	94	89	96	152	211	276	287	247
134	162	162	143	120	102	94	89	96	124	169	191	171	150	122	100	91	124	276	299	299	299	255
140	172	163	144	118	99	90	89	97	135	177	192	172	149	121	100	96	149	299	299	299	299	255
104	110	108	103	95	94	88	87	86	103	117	121	117	108	99	90	91	123	294	299	299	299	255
90	87	87	85	87	91	84	87	87	88	91	91	90	89	89	88	89	108	144	177	172	172	144
86	87	85	83	83	83	85	86	87	88	86	87	85	86	87	85	94	108	119	126	118	110	97
86	84	81	85	84	85	87	87	85	86	87	85	87	89	85	91	96	113	117	113	112	102	95
89	87	85	85	85	83	87	85	85	87	89	87	87	89	85	91	109	116	112	109	100	95	93
85	86	85	85	83	86	85	81	83	84	85	83	81	83	91	97	103	109	105	99	95	91	86
Background area 2																	Background area 4					

Dynamic mask image: −1 = rejected; 0 = background; 1 = peak

0	0	0	0	0	0	0	0	0	0	0	0	0	0	0	0	0	0	0	0	0	0	0
0	0	0	0	0	0	0	0	0	0	0	0	0	0	0	0	0	0	0	0	0	0	0
0	0	0	0	0	0	0	0	0	0	0	0	0	0	0	0	0	0	0	0	0	−1	−1
0	0	0	0	0	0	0	0	0	0	0	1	1	0	0	0	0	0	0	−1	−1	−1	−1
0	−1	−1	−1	0	0	0	0	0	1	1	1	1	1	1	0	0	0	−1	−1	−1	−1	−1
−1	−1	−1	−1	−1	0	0	0	1	1	1	1	1	1	1	1	0	−1	−1	−1	−1	−1	−1
−1	−1	−1	−1	−1	0	0	0	1	1	1	1	1	1	1	1	1	−1	−1	−1	−1	−1	−1
−1	−1	−1	0	0	0	0	0	1	1	1	1	1	1	1	0	0	−1	−1	−1	−1	−1	−1
0	0	0	0	0	0	0	0	0	0	0	0	0	0	0	0	0	0	−1	−1	−1	−1	−1
0	0	0	0	0	0	0	0	0	0	0	0	0	0	0	0	0	0	−1	−1	−1	−1	−1
0	0	0	0	0	0	0	0	0	0	0	0	0	0	0	0	0	0	−1	−1	−1	−1	0
0	0	0	0	0	0	0	0	0	0	0	0	0	0	0	0	0	0	−1	−1	−1	0	0
0	0	0	0	0	0	0	0	0	0	0	0	0	0	0	0	0	0	−1	0	0	0	0

area detector, these authors chose to collapse the three-dimensional image to two dimensions, thus losing some of the advantages which the peak fitting techniques provide (Spencer, 1980). In addition, spot shapes are often quite difficult to describe by a simple function, especially for X-ray films taken with a synchrotron source, in which case they depend mostly on crystal shapes. In these cases describing the spots by a general and continuously changing mask is much to be preferred.

The dynamic mask procedure offers an additional possibility of calculating one-dimensional projections of reflection data originally collected with two- and three-dimensional techniques. Such projections can be calculated on the basis of net intensities after background subtraction and, in that case, do not lead to any loss of statistical significance. On the other hand, such data can be used to extract useful intensities even from partially overlapping reflections, enabling us to deal more easily with crystals having larger unit cells. This aspect of the work will be described elsewhere.

We would like to thank Drs S. Spencer and A. Kossiakoff for communicating their results prior to publication and for stimulating discussions. We are indebted to Professor O. Lindqvist for fruitful suggestions and for his interest in this work and to Drs R. Bott and M. Navia for providing us with the films used in this study.

References

ABRAHAMSSON, S. (1969). *J. Sci. Instrum.* **43**, 931–933.

ABRAHAMSSON, S., KIERKEGAARD, P., ANDERSSON, E., LINDQVIST, O., LUNDGREN, G. & SJÖLIN, L. (1980). *J. Appl. Cryst.* **13**, 318–337.

ABRAHAMSSON, S., LINDQVIST, O., SJÖLIN, L. & WLODAWER, A. (1981). *J. Appl. Cryst.* In the press.

ALEXANDER, L. E. & SMITH, G. S. (1964). *Acta Cryst.* **17**, 1195–1201.

ARNDT, U. W. & WONACOTT, A. J. (1977). *The Rotation Method in Crystallography*. Amsterdam: North Holland.

BLESSING, R. H., COPPENS, P. & BECKER, P. (1974). *J. Appl. Cryst.* **7**, 488–492.

CORNICK, G. & NAVIA, M. A. (1980). Private communication.

DIAMOND, R. (1969). *Acta Cryst.* A**25**, 43–55.

FORD, G. C. (1974). *J. Appl. Cryst.* **7**, 555–564.

GRANT, D. F. & GABE, E. J. (1978). *J. Appl. Cryst.* **11**, 114–120.

HAMILTON, W. C., ROLLETT, J. S. & SPARKS, R. A. (1965). *Acta Cryst.* **18**, 129–130.

KABSCH, W. (1977). *J. Appl. Cryst.* **10**, 426–429.

LEHMANN, M. S. (1975). *J. Appl. Cryst.* **8**, 619–622.

LEHMANN, M. S. & LARSEN, F. K. (1974). *Acta Cryst.* A**30**, 580–584.

MATTHEWS, B. W., KLOPFENSTEIN, C. E. & COLMAN, P. M. (1972). *J. Phys. E*, **5**, 353–359.

NOCKOLDS, C. E. & KRETSINGER, R. M. (1970). *J. Phys. E*, **3**, 842–846.

PHEARSON, R. H. (1975). *Acta Cryst.* A**31**, S236.

PRINCE, E., WLODAWER, A. & SANTORO, A. (1978). *J. Appl. Cryst.* **11**, 173–178.
ROSSMANN, M. G. (1979). *J. Appl. Cryst.* **12**, 225–238.
SANTORO, A. & WLODAWER, A. (1980). *Acta Cryst.* A**36**, 440–450.
SJÖLIN, L., OLSSON, G. & LINDQVIST, O. (1975). *J. Appl. Cryst.* **8**, 678–680.
SLAUGHTER, M. (1969). *Z. Kristallogr.* **129**, 369–380.
SPENCER, S. (1980). Private communication.
SPENCER, S. & KOSSIAKOFF, A. (1980). *J. Appl. Cryst.* **13**, 563–571.
WERNER, P. E. (1969). *Ark. Kem.* **31**, 505–516.
WLODAWER, A. (1974). *J. Appl. Cryst.* **7**, 19–21.
WLODAWER, A. (1980). *Acta Cryst.* B**36**, 1826–1831.
WLODAWER, A. & SJÖLIN, L. (1981). In preparation.
XUONG, N.-H. (1969). *J. Phys. E*, **2**, 485–489.
XUONG, N.-H., FREER, S. T., HAMLIN, R., NIELSEN, C. & VERNON, W. (1978). *Acta Cryst.* A**34**, 289–296.

SHORT COMMUNICATION

Contributions intended for publication under this heading should be expressly so marked; they should not exceed about 1000 *words; they should be forwarded in the usual way to the appropriate Co-editor; they will be published as speedily as possible.*

Acta Cryst. (1981). A**37**, 604

Piezoelectric effect in $CdCl_2.2NiCl_2.12H_2O$.

By H.-D. MAURY, H. BÖHM and W. FISCHER,* *Institute für Mineralogie der Universität, D-4400 Münster, Federal Republic of Germany*

(*Received* 5 *November* 1979; *accepted* 13 *February* 1981)

Abstract

For the double salt $CdCl_2.2NiCl_2.12H_2O$ the piezoelectric modulus d_{33} was measured to prove the lack of a center of symmetry. From the result of this experiment, the space group $P3$ can be attributed to this compound.

The double salt $CdCl_2.2NiCl_2.12H_2O$ is reported to belong to space group $P\bar{3}$ (*e.g.* Gmelin, 1966). Apparently, the assumption of space group $P\bar{3}$ originates from the crystal structure investigation of Ferrari & Cavalca (1946) who favored this space group. Later attempts to determine the structure failed, because the refinement calculations in neither $P\bar{3}$ nor in $P3$ lead to a satisfactory coincidence between calculated and observed intensities (Koch & Fischer, 1977). In order to check the absence of a center of symmetry, measurements of the piezoelectric effect were carried out on this compound.

The crystals were grown from aqueous solution. According to the method described by Gmelin (1966) an excess of $NiCl_2$ was added to guarantee that only the stable compound of $CdCl_2.2NiCl_2.12H_2O$ precipitated. Crystallization occurred after 28 d yielding green hexagonal platelets of 1 to 8 mm in diameter.

The table of piezoelectric moduli (Voigt, 1910) shows that there are six independent and non-vanishing moduli in the point group 3. In particular, a stress which is applied parallel to any of the crystallographic axes will produce a polarization parallel to itself. Since the crystals were grown as platelets with the main face perpendicular to the c axis, it seemed reasonable to measure the polarization P_3 parallel to **c**. In the two-suffix notation the component P_3 is given by

$$P_3 = d_{33}\sigma_3,$$

where d_{33} = piezoelectric modulus, σ_3 = stress component parallel to **c**.

For the measurements the faces were coated with silver paste and the experiment was carried out in a dry argon atmosphere to prevent the surface charge being affected by humidity. The device used will be described elsewhere. The measurements were carried out in a dynamic and a static experiment.

In the dynamic experiment, after Bergmann (1935), the crystal was excited into a longitudinal vibration by an electrodynamic vibrator. The AC signal which is produced by the piezoelectric effect at the electrodes is fed into a lock-in amplifier which also drives the vibrator. The amplified AC signal is depicted on the screen of an oscilloscope. For the double salt $CdCl_2.2NiCl_2.12H_2O$ a strong AC signal is observed which is even stronger than that of a comparable sample of quartz. This strong piezoelectric effect proves the lack of a center of symmetry.

In the static experiment a stress was applied to the crystal by a known force F causing a polarization. The surface charge Q was measured with an electrometer. The piezoelectric modulus d is determined by the relation

$$d = Q/F.$$

For $CdCl_2.2NiCl_2.12H_2O$ the modulus d_{33} was measured.

$$d_{33} = (9{\cdot}130 \pm 0{\cdot}007) \times 10^{-12}\ \mathrm{CN}^{-1}.$$

From the strong piezoelectric effect we therefore must conclude that $CdCl_2.2NiCl_2.12H_2O$ belongs to space group $P3$.

References

BERGMANN, L. (1935). *Z. Phys.* **36**, 31–34.
FERRARI, A. & CAVALCA, L. (1946). *Rend. Soc. Mineral. Ital.* **3**, 117–120.
GMELIN (1966). *Gmelins Handbuch der anorganische Chemie*. Weinheim: Verlag Chemie GmbH.
KOCH, E. & FISCHER, W. (1977). Private communication.
VOIGT, W. (1910). *Lehrbuch der Kristallphysik*, p. 130. Stuttgart: Teubner Verlagsgesellschaft.

* Present address: Institut für Kristallographie der Universität, D-3550 Marburg, Federal Republic of Germany.

0567-7394/81/040604-01$01.00